Alma Mater Studiorum Università di Bologna
Archivio istituzionale della ricerca

Inverted Ligand Field in a Pentanuclear Bow Tie Au/Fe Carbonyl Cluster

(Article begins on next page)

06 October 2024

Inverted Ligand Field in penta-nuclear tie-bow Au/Fe carbonyl cluster

Gabriele Manca,[1,*] Fabrizia Fabrizi de Biani,[2] Maddalena Corsini,[2] Cristiana Cesari,[3] Cristina Femoni,[3] Maria Carmela Iapalucci,[3,*] Stefano Zacchini,[3] Andrea Ienco.[1]

[1] Istituto di Chimica dei Composti Organometallici (CNR-ICCOM), 50019, Sesto Fiorentino, Italy.

[2] Dipartimento di Chimica Industriale "Toso Montanari", Università di Bologna, Viale Risorgimento 4, 40136 Bologna, Italy.

[3] Dipartimento di Biotecnologie Chimica e Farmacia and C.I.R.C.M.S.B., Università di Siena Via Aldo Moro, 53100 Siena, Italy.

Corresponding authors: gabriele.manca@iccom.cnr.it; maria.iapalucci@unibo.it.

Abstract

Gold chemistry has experienced in the last decades an exponential attention for a wide spectrum of chemical applications, but +III oxidation state, traditionally assigned to gold, remains somewhat questionable. Herein, we present a detailed analysis of the electronic structure of the pentanuclear tie-bow Au/Fe carbonyl cluster $[Au\{\eta^2\text{-}Fe_2(CO)_8\}_2]^-$ together with its two one-electron reversible reductions. A new interpretation of the bonding pattern is provided with the help of the Inverted Ligand Field Theory. The classical view of a central gold (III) interacting with two $[Fe_2(CO)_8]^{2-}$ units is replaced by Au(I), d^{10} gold configuration, with two interacting $[Fe_2(CO)_8]^-$ fragments. A d^{10} configuration for the gold center in the compound $[Au\{\eta^2\text{-}Fe_2(CO)_8\}_2]^-$ is confirmed by the LUMO orbital composition, mainly localized on the iron carbonyl fragments rather than on a d gold orbital, as expected for a d^8 configuration. Upon one-electron stepwise reduction, the spectroelectrochemical measurements show a progressive red shift in the carbonyl stretching, in agreement with the increased population of the LUMO centered on the iron units. Such a trend is also confirmed by the X-ray structure of the di-reduced compound $[Au\{\eta^1\text{-}Fe_2(CO)_8\}\{\eta^2\text{-}Fe_2(CO)_6(\mu\text{-}CO)_2\}]^{3-}$, featuring the cleavage of one Au-Fe bond.

1. INTRODUCTION

For many years, the development of homogeneous gold-based catalysts[1-5] has been hampered due to a somewhat recalcitrance of gold complexes to undergo the most common processes of coordination chemistry, such as oxidative addition and reductive elimination.[1,6] Only in the recent years, gold chemistry has experienced a renewed interest pushed by the ubiquitous employment of both gold complexes and nanoparticles in nano-medicine,[7-9] sensors[10,11] and catalysis,[2-5] as well as environmental applications.[12] Moreover, in many catalytic cycles, the involvement of Au(III) intermediates is suggested.[2-5]

Recently, the possible +1/+3 oxidation of some XI group square planar complexes has been largely debated and reviewed, especially in the case of copper complexes. In this regards, particular attention was devoted toward the $[Cu(CF_3)_4]^-$ square planar complex[13-15] for which, according to the classical Ligand Field (LF) theory, a formal +III oxidation state (metal d^8 configuration) is attributed to Cu surrounded by four CF_3^- anions, in a square planar arrangement. The bonding description of such a complex has been strongly debated until the early 90's, when Snyder raised some doubts on the assigned oxidation state.[16] According to Snyder, an oxidation state +I should be assigned to Cu surrounded by three CF_3 anions and one CF_3^+ cation. Snyder's hypothesis was fiercely criticized [17] for the unrealistic presence of a trifluoromethylcation in the complex. A recent review provides a complete picture of the electronic distribution in the complex through a detailed analysis of the interaction between the combinations of the ligand sets and the d orbitals of the metal.[18] In the traditional LF, all the interactions are classified as electron donations from the ligands to the empty metal orbitals. Conversely, the bonding in $[Cu(CF_3)_4]^-$ can be described as formed by three electron-pair donations from the ligand combinations into the empty s/p metal orbitals, and by a σ donation from the occupied metal orbital into a vacant combination of the ligands.[18] The presence of a combination of the ligand orbitals higher in energy than the d-metal orbitals reverts the classic Ligand Field (LF) description.[19-21]

The Inverted Ligand Field (ILF) theory has been confirmed by detailed spectroscopic and X-ray analysis.[14,18] Scheme 1 highlights the differences between the classic LF and ILF. In ILF, one bonding orbital has a prominent contribution from the metal while the anti-bonding counterpart, usually the LUMO, is centered on the ligands. Thus, the electronic population is inverted, going from the metal to the ligand. The analysis of the metal and ligand contributions in the anti-bonding orbitals is a diagnostic tool for the occurrence of ILF.[14,18,22,23]
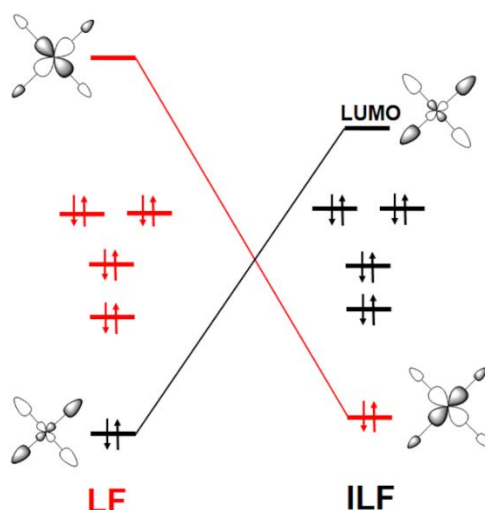
Scheme 1. Simplified picture of molecular orbitals involving metal d orbitals in: Ligand Field (LF) description on the left and Inverted Ligand Field (ILF) on the right.

A combined experimental/computational investigation was extended to other Cu(III) complexes and compared with Cu(II) paramagnetic species.[22] The result was the extension of the ILF to other cases, traditionally proposed as Cu(III) complexes. A similar bonding pattern has been found also in Au(III) complexes bearing CF_3 ligands.[23-25]

A deep understanding of the electronic structure is not only useful for metal complexes but also for small clusters,[26,27] since it may open or predict new synthetic pathways or catalytic cycles.[28,29] In this regards, some years ago the bimetallic Au/Fe tie-bow pentanuclear cluster $[Au\{\eta^2\text{-}Fe_2(CO)_8\}_2]^-$ [30-33] was synthesized; this features a central gold atom surrounded by two $Fe_2(CO)_8$ units (from now on indicated as Fe_2), in a square planar coordination. The cluster may undergo two reversible one-electron reductions with the final formation of a tri-anionic species. According to the traditional rules, in the parent tie-bow $[Au\{\eta^2\text{-}Fe_2(CO)_8\}_2]^-$ cluster a formal oxidation state +III was assigned to the gold center with two $[Fe_2(CO)_8]^{2-}$ units. Accordingly, the two-sequential reduction processes involved the gold center up to the achievement of Au(I) d^{10} configuration.

In the present article, an innovative description of the bonding is proposed, based on the Inverted Ligand Field theory with the assignment of d^{10} electron configuration to gold and with the two $[Fe_2(CO)_8]^-$ units. Furthermore, the redox behavior has been reinterpreted, also taking into account the X-ray structure of the di-reduced trianionic cluster. This computational/experimental approach

represents the first case of the application of the ILF theory to a metal cluster, and a step toward the clear understanding of coinage metals cluster and nanoparticles formation pathways.

2. EXPERIMENTAL SECTION

2.1 Synthesis of [NEt$_4$]$_3$[Au{η^1-Fe$_2$(CO)$_8$}{η^2-Fe$_2$(CO)$_6$(μ-CO)$_2$}]. A solution of Na-naphtalenide (0.63 M in THF, 2.80 mL, 1.76 mmol) was added to a solution of [NEt$_4$][Au{η^2-Fe$_2$(CO)$_8$}$_2$] (0.870 g, 0.871 mmol) in THF (20 mL) at -70 °C. The solution was warmed up to room temperature with stirring, then the solvent was removed under reduced pressure. The residue was dissolved in CH$_3$CN (15 mL), the solution filtered off and layered with n-hexane (3 mL) and di-iso-propyl-ether (40 ml) affording crystals of [NEt$_4$]$_3$[Au{η^1-Fe$_2$(CO)$_8$}{η^2-Fe$_2$(CO)$_6$(μ-CO)$_2$}] suitable for single crystal X-ray diffraction (yield 0.21 g, 19%).

2.2 Infrared spectroelectrochemistry

Infrared spectroelectrochemistry (IR-SEC) experiments were performed using a 10 mM solution of the complex in MeCN or THF, containing 0.2 M TBAPF$_6$ as supporting electrolyte. The experiments were carried out in a LabOMak UF-SEC cell with Pt mesh working and counter electrode. The working electrode potential was varied from –0.40 V to –0.60 V and then from –0.60 V to –0.75 V *vs*. pseudo-Ag electrode (step potential 5 mV). Details of materials and apparatus for electrochemistry have been described elsewhere.[34]

2.3 X-ray Crystallography. Crystal data and collection details for [NEt$_4$]$_3$[Au{η^1-Fe$_2$(CO)$_8$}{η^2-Fe$_2$(CO)$_6$(μ-CO)$_2$}] are reported in Table 1. Data were collected on a Bruker Apex II diffractometer using graphite monochromated MoK$_\alpha$ radiation (λ = 0.71073 Å) at room temperature. The structure was solved by Direct Methods and refined by full-matrix least-squares based on all data using F^2.[35] All non-hydrogen atoms were refined anisotropically, while hydrogen atom positions were set geometrically.

Table 1. Crystal structure data for **[NEt$_4$]$_3$[Au{η^1-Fe$_2$(CO)$_8$}{η^2-Fe$_2$(CO)$_6$(μ-CO)$_2$}]**

Compound	C$_{40}$H$_{60}$AuFe$_4$N$_3$O$_{16}$
Fw	1259.27
T, K	296(2) K

λ, Å	0.71073 A
Crystal system	Monoclinic
Space group	$P2_1/c$
a, Å	9.6325(6)
b, Å	47.195(3)
c, Å	11.7532(8)
α, °	90
β, °	113.8360(10)
γ, °	90
Cell Volume, Å^3	4887.3(5)
Z	4
D_c, g cm^{-3}	1.711
μ, mm^{-1}	4.218
F(000)	2528
Crystal size, mm	0.30 x 0.15 x 0.15
θ limits, °	1.726 to 25.098
Index ranges	−11<=h<=11, −56<=k<=56, −14<=l<=14
Reflections collected	47658
Independent reflections	8697 [R(int) = 0.0914]
Completeness to $\theta = 25.00°$	99.9 %
Data / restraints / parameters	8697 / 0 / 589
Goodness on fit on F^2	1.038
R_1 ($I > 2\sigma(I)$)	0.0449
wR_2 (all data)	0.1010
Largest diff. peak and hole, e Å^{-3}	1.138 and −0.595

2.4 Computational details

All the compounds were optimized at DFT-B3LYP[36] level of theory within the Gaussian 16 package.[37] All the calculations were based on the CPCM model[38,39] for the TetraHydroFuran as solvent, the same used in the experimental conditions. The Triple Zeta basis set TZVP[40] was used for all the atomic species, except for the Gold and Iodine atoms, for which the Stuttgart/Dresden (SDD) *pseudo*-potential[41] was employed. All the optimized structures were validated as minima by computing vibrational frequencies. The contribution of each center to the molecular orbitals was

estimated by using the AOMIX package.[42,43]Cartesian coordinates as well as the energetic features of all the optimized structures are reported in the Supporting Info.

3.RESULTS AND DISCUSSION

3.1 Chemical Reduction of $[Au\{\eta^2\text{-}Fe_2(CO)_8\}_2]^-$ and Synthesis of $[Au\{\eta^2\text{-}Fe_2(CO)_8\}\{\eta^2\text{-}Fe_2(CO)_6(\mu\text{-}CO)_2\}]^{2\text{-}\bullet}$ and $[Au\{\eta^1\text{-}Fe_2(CO)_8\}\{\eta^2\text{-}Fe_2(CO)_6(\mu\text{-}CO)_2\}]^{3\text{-}}$.

The red $[Au\{\eta^2\text{-}Fe_2(CO)_8\}\{\eta^2\text{-}Fe_2(CO)_6(\mu\text{-}CO)_2\}]^{2\text{-}\bullet}$ dianion and red-brown $[Au\{\eta^1\text{-}Fe_2(CO)_8\}\{\eta^2\text{-}Fe_2(CO)_6(\mu\text{-}CO)_2\}]^{3\text{-}}$ trianion are obtained by reduction of the green $[NEt_4][Au\{\eta^2\text{-}Fe_2(CO)_8\}_2]$ salt at -70°C in THF with *ca.* one and two equivalents of Na-naphtalenide, respectively, while monitoring the reduction *via* IR spectroscopy. As previously reported,[32] upon addition of the first equivalent of Na-naphtalenide, the solution turns from green to red, and its IR spectrum shows the presence of $[Au\{\eta^2\text{-}Fe_2(CO)_8\}\{\eta^2\text{-}Fe_2(CO)_6(\mu\text{-}CO)_2\}]^{2\text{-}\bullet}$, characterized carbonyl absorptions at 2018(w), 2000(sh), 1984(ms), 1942(s) and 1767(ms) cm^{-1}. Then, after addition of a second equivalent of Na-naphtalenide, $[Au\{\eta^2\text{-}Fe_2(CO)_8\}\{\eta^2\text{-}Fe_2(CO)_6(\mu\text{-}CO)_2\}]^{3\text{-}}$ is formed and it displays an IR pattern similar to the dianion, with carbonyl absorptions at 1970(ms), 1930(s) and 1860(m) cm^{-1}. Addition of further Na-naphtalenide causes the progressive decomposition of the Au-Fe trianion and leads to the formation of $[Fe_2(CO)_8]^{2\text{-}}$ and $[Fe(CO)_4]^{2\text{-}}$, which become the only detectable carbonyl products after addition of 3-4 equivalents of Na-naphtalenide. Both the first and particularly the second reduction in THF are accompanied by separation of some precipitate. Therefore, both suspensions have been evaporated to dryness and the residues have been dissolved in acetonitrile. All attempts to isolate crystals of the dianion from the above acetonitrile solutions failed, owing to formation of an amorphous precipitate in mixture with few crystals of the starting $[NEt_4][Au\{\eta^2\text{-}Fe_2(CO)_8\}_2]$ salt. Interestingly, warming up of the purple solution of $[Au\{\eta^2\text{-}Fe_2(CO)_8\}\{\eta^2\text{-}Fe_2(CO)_6(\mu\text{-}CO)_2\}]^{3\text{-}}$ leads to a great change in the IR pattern of the carbonyl absorptions. Nevertheless, a trianion has been isolated in very low yields by layering of *n*-hexane and di-iso-propyl-ether on top of its acetonitrile solution. A X-ray structural determination of its $[NEt_4]^+$ salt (see next) unexpectedly disclosed that the gold atom of the trianion is only tri- rather than tetra-coordinated by iron. This finding seemed to challenge the reversibility of the redox

changes, which should imply absence of gross structural changes and prompted further electrochemical and spectroelectrochemical investigations.

3.2 Spectroelectrochemical investigation of the reduction of $[Au\{\eta^2\text{-}Fe_2(CO)_8\}_2]^-$.

The tie-bow pentanuclear cluster undergoes two reversible one-electron reductions at -0.68 and -0.89 V (*vs.* SCE) in THF solution (Figure S1). These reduction processes are followed by a couple of more cathodic irreversible processes (at -2.1 V and -2.3 V), as previously described in literature.[30,31]

Due to the low solubility of the reduced species, the UV-vis spectroelectrochemistry (Figure S2) is not highly informative since the main feature is the disappearance of the intense band centered at 750 nm, observed upon the reduction of the monoanion.

The separation of a precipitate, due to the reduction process, causes some difficulties also in the IR spectroelectrochemical study of $[Au(\eta^2\text{-}Fe_2(CO)_8)_2]^-$, both in THF and MeCN solutions, even if better results are obtained in MeCN. Figure 1 shows the spectral changes accompanying the step-by-step reduction of the monoanion in MeCN. Apparently, the absence of signals in the edge-bridging region in the initial spectrum, suggests that in these experimental conditions the equilibrium of the monoanionic isomers is driven toward the one with all terminal carbonyls. Anyway, as expected, after the addition of one electron a signal in the edge-bridging region appears at 1755 cm^{-1}, while the ν_{CO} group of bands, relative to the terminal carbonyls, is red-shifted. The addition of a further electron is accompanied by a similar red shift of both the terminal and the edge-bridging ν_{CO} bands. Even if the edge-bridging ν_{CO} frequencies are less evident in THF, the general behaviour is similar both in MeCN and in THF, as shown by the values in Table 2, reporting all the ν_{CO} IR frequencies of the mono-, di- and trianion in both solvents. Oxidation of both the di- and trianion allows to recover the original spectrum, even if its intensity is lower in view of its partial precipitation. Thus, for each redox state an equilibrium may exist between a scarcely soluble species and a soluble one. The latter can be reversibly re-oxidised to the original compound. The bulk electrolysis of a MeCN solution of $[Au(\eta^2\text{-}Fe_2(CO)_8)_2]^-$ provides a similar result. The cyclic voltammograms of both the di- and trianionicelectrogenerated species are complementary to the initial one, but for the lower current intensity, which is also due to the lower concentration, remained in solution after the one- and two-electron reduction of the cluster. While

do not allowing the direct observation of the trianionic cluster with tri-coordinated gold, all together these results would match with the hypothesis that this could be the low-soluble component, which for this reason is not observed neither by electrochemistry nor by spectroelectrochemistry.
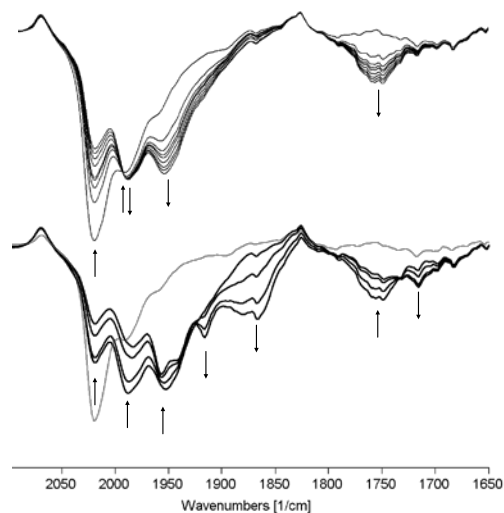

Figure 1. Infrared spectra recorded in an OTTLE cell during the stepwise overall reduction of $[Au(\eta^2\text{-}Fe_2(CO)_8)_2]^-$ $(0.9 \times 10^{-3}$ M) in MeCN solution $([NEt_4][PF_6]$ (0.10 M) as supporting electrolyte). Top: first reduction: E_w from –0.40V to –0.60 V, *vs*. pseudo-Ag electrode; bottom: second reduction: E_w from –0.60 V to –0.75 V, *vs*. pseudo-Ag electrode, grey line: initial spectrum.

Table 2. IRν_{CO} frequencies for the differently charged cluster, observed during spectroelectrochemistry.

	MeCN	THF
monoanion	2019, 1990, 1959	2016, 1990, 1957
dianion	1988, 1952, 1755	1986, 1954, 1940, 1770, 1742
trianion	1916, 1866, 1717	1910, 1867, 1717

3.2 Structure of $[Au\{\eta^1\text{-}Fe_2(CO)_8\}\{\eta^2\text{-}Fe_2(CO)_6(\mu\text{-}CO)_2\}]^{3-}$.

The structure of $[Au\{\eta^1\text{-}Fe_2(CO)_8\}\{\eta^2\text{-}Fe_2(CO)_6(\mu\text{-}CO)_2\}]^{3-}$ is shown in Figure 2 and the intermetallic distances are collected in Table 3 and compared with those of the monoanionic species. All the other bond lengths of the trianionic structure are reported in Table S1.

As illustrated in Figure 2, the unique Au atom of $[Au\{\eta^1\text{-}Fe_2(CO)_8\}\{\eta^2\text{-}Fe_2(CO)_6(\mu\text{-}CO)_2\}]^{3-}$ (formally Au(I)) is tri- rather than tetra-coordinated, differently from the $[Au\{\eta^2\text{-}$

Fe$_2$(CO)$_8$}$_2$]$^-$ and [Au{η^2-Fe$_2$(CO)$_8$}{η^2-Fe$_2$(CO)$_6$(μ-CO)$_2$}]$^-$ isomeric square-planar mono-anions. Its metal framework can be derived from the latter one by breaking one of the two Au-Fe bonds connecting the Fe$_2$(CO)$_8$ moiety (with only terminal carbonyl groups) to the central Au atom. Indeed, the Au-Fe(5) interatomic separation [4.452(1) Å] is well beyond the sum of the van der Waals radii of iron and gold. This gives rise to a dangling Fe(CO)$_4$ moiety which displays a trigonalbipyramidal rather than an octahedral stereochemistry.

To the best of our knowledge, there are not previously reported examples of pentanuclear clusters displaying a similar metal framework. Perhaps, the only related example is Ru$_5$(CO)$_{16}$(μ-PPh$_2$)(μ_5-P).[44]

It is worth mentioning that localized breaking of one M-M bond upon addition of 2 electrons is neither surprising nor exceptional in cluster chemistry. What is perhaps more surprising is that the sacrificed M-M bond is an Au-Fe rather than a Fe-Fe bond, as documented, for instance, by the structures of the neutral [M(Fe$_2$(CO)$_8$)$_2$] and the dianionic [M(Fe$_2$(CO)$_8$)$_2$]$^{2-}$ (M = Sn, Pb). It seems reasonable to suggest that such a difference is mainly due to a more favorable sp^2 hybridization of Au(I).

As expected, the Fe(2)-Fe(3) contact [2.6094(13) Å] bridged by two CO ligands is shorter than Fe(4)-Fe(5) [2.8763(13) Å] which display only terminal carbonyls. Due to the increased negative charge of the cluster, both CO bridged and unbridged Fe-Fe contacts are significantly elongated compared to those found in the isomeric monoanions [Au{η^2-Fe$_2$(CO)$_8$}$_2$]$^-$ and [Au{η^2-Fe$_2$(CO)$_8$}{η^2-Fe$_2$(CO)$_6$(μ-CO)$_2$}]$^-$ [2.764-2.771 Å for all terminal moieties, 2.571-2.574 Å in the presence of μ-CO].[32] A similar elongation is observed for the Au-Fe contacts of [Au{η^1-Fe$_2$(CO)$_8$}{η^2-Fe$_2$(CO)$_6$(μ-CO)$_2$}]$^{3-}$ [2.6502(9)-2.7290(9) Å] compared to [Au{η^2-Fe$_2$(CO)$_8$}$_2$]$^-$ [2.583-2.607 Å] and [Au{η^2-Fe$_2$(CO)$_8$}{η^2-Fe$_2$(CO)$_6$(μ-CO)$_2$}]$^-$ [2.588-2.620 Å]. Such Au-Fe distances are in keeping with those found in other Au-Fe carbonyl clusters containing Au in the formal oxidation state +1.[45-47]
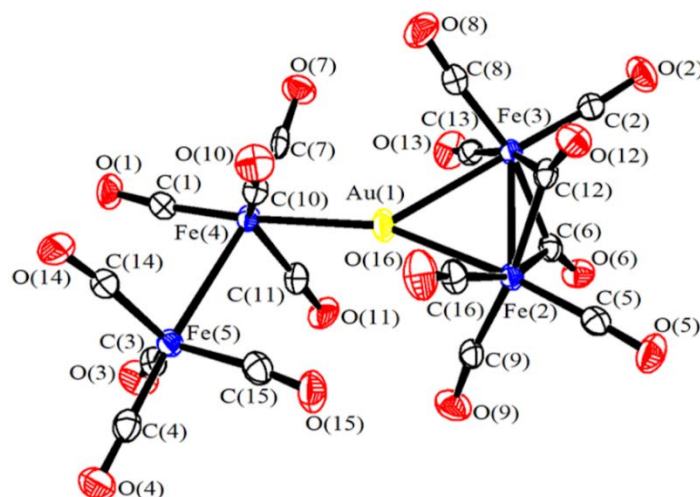
Figure 2. Molecular structure of $[Au\{\eta^1\text{-}Fe_2(CO)_8\}\{\eta^2\text{-}Fe_2(CO)_6(\mu\text{-}CO)_2\}]^{3-}$ with labeling. Thermal ellipsoids are at the 30% probability level.

Table 3. Comparison of the Au-Fe and Fe-Fe bond lengths (Å) of $[Au\{\eta^1\text{-}Fe_2(CO)_8\}\{\eta^2\text{-}Fe_2(CO)_6(\mu\text{-}CO)_2\}]^{3-}$ (**A**), $[Au\{\eta^2\text{-}Fe_2(CO)_8\}_2]^-$ (**B**) and $[Au\{\eta^2\text{-}Fe_2(CO)_8\}\{\eta^2\text{-}Fe_2(CO)_6(\mu\text{-}CO)_2\}]^-$ (**C**). Labeling from Figure 2.

	A	**B** [a]	**C** [a,b]	**C** [a,c]
Au(1)-Fe(2)	2.6502(9)	2.607	2.596	2.591
Au(1)-Fe(3)	2.7290(9)	2.583	2.602	2.623
Au(1)-Fe(4)	2.6173(9)	2.607	2.584	2.585
Au(1)-Fe(5)	4.452(1)	2.583	2.595	2.618
Fe(2)-Fe(3)	2.6094(13) [d]	2.771 [e]	2.574 [d]	2.571 [d]
Fe(4)-Fe(5)	2.8763(13) [e]	2.771 [e]	2.765 [e]	2.764 [e]

[a] Data from references 30-32. [b] As $[NEt_4]^+$ salt. [c] As diethylviologen salt. [d] Fe-Fe bridged by two μ-CO ligands. [e] Unbridged Fe-Fe.

3.4 Reinterpretation of bonding by Inverted Ligand Field

Pentanuclear clusters are known with a large variety of structural arrangements.[48,49] One of the latter, although not so usual, exhibits a tie-bow geometry, featuring a central metal atom linked to other four, thus forming two triangles sharing a vertex. One example is the pentanuclear $[Os_5(CO)_{19}]$ featuring a central $Os(CO)_3$ moiety linked to two $[Os_2(CO)_8]$ units with a total valence electron count of 78.[50] The cluster is obtained through thermal treatment of the octahedral $[Os_6(CO)_{18}]$ homonuclear cluster, under CO atmosphere. Among the methods developed in the years for the prediction of the structure and the bonding in the transition metal clusters, one of the

simplest is the electron counting actuated by using the empirical equations, shown in Eqs. 1. The two variables are the number of total linkages (m) and the lone pairs (n) on the transition metal centers with the basic assumption that each of the nine valence orbitals of the metals (five d, one s and three p type) is involved in the bonding or occupied by a lone pair.[51,22]

$$2m + n = \text{number of the orbitals} \qquad \text{Eqs. 1}$$

$$2m+2n = \text{number of the electrons}$$

In $[Os_5(CO)_{19}]$, the total number of orbitals is 64, 45 of which coming from the metal (nine for each osmium center) and 19 from the ligands (one for each CO). The total electron count is 78, considering each CO as a 2e$^-$ donor. Thus, the exact solutions of the equations 1 are n=14, lone pairs, and m= 25 bonds, 19 of which are the Os-CO bonds while the remaining 6 are the Os-Os linkages (correctly predicted). The 14 lone pairs are distributed as follows: three for each of the $Os(CO)_4$ fragment of the $Os_2(CO)_8$ units and two for the central $Os(CO)_3$ one.

The equations 1 have been applied also for the prediction of the M-M linkages and lone pairs for the present tie-bow pentanuclear cluster $[Au\{\eta^2\text{-}Fe_2(CO)_8\}_2]^-$. The latter has a total electron count of 76 e$^-$ and 61 orbitals, thus the corresponding solutions of the equations 1 are n= 15 lone pairs and m=23 linkages, 16 of which are M-CO bonds, thus 7 M-M bonds are predicted for the cluster. In this case, a discrepancy occurred between the value n=7, predicted by equations 1 and the 6 M-M bonds, experimentally observed. Eventually, this discrepancy will be explained later.

A detailed computational analysis has been carried out starting from the optimization of the two isomeric structures of the monanionic pentanuclear clusters $[Au\{\eta^2\text{-}Fe_2(CO)_8\}_2]^-$, shown in Figure 3 (a) without and b) with two bridging CO ligands). The optimized structures nicely reproduce the available X-ray ones, except for a somewhat elongation of the metal-metal distances (less than 0.1 Å, as shown in Table S2). A similar trend is well reported in literature and it is reasonable due to the employment of a *pseudo*-potential for the metal centers.[53,54] Both structures feature a distorted octahedral arrangement around each Fe center and a square planar coordination at Au.[31,32] From an energy viewpoint, the second isomer, with bridging CO in Figure 3b, is practically equivalent in free energy to the unbridged one, being less stable by 1.5 kcal mol^{-1}.
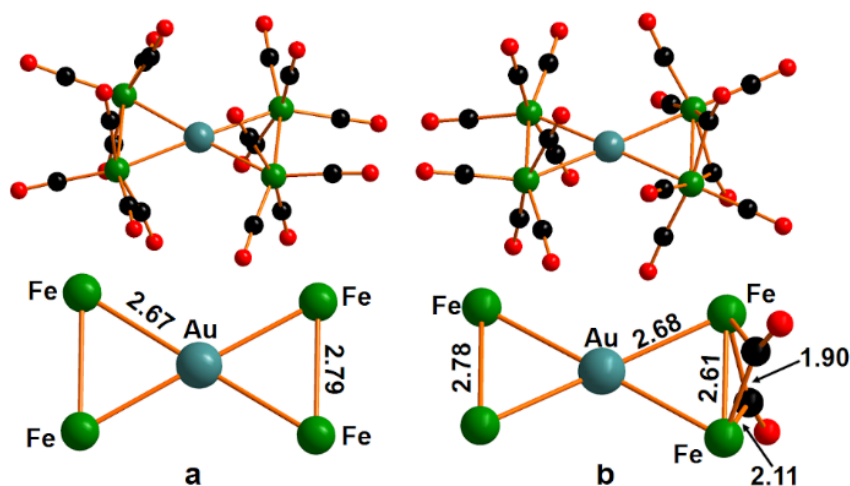
Figure 3. Upper part. Optimized structure of the: a) $[Au\{\eta^2\text{-}Fe_2(CO)_8\}_2]^-$ without bridging CO ligands and b) $[Au\{\eta^2\text{-}Fe_2(CO)_8\}\{\eta^2\text{-}Fe_2(CO)_6(\mu\text{-}CO)_2\}]^-$ with two bridging COs. Lower part. Simplified scheme of M-M distance and bridging ligands where available

The calculated IR spectrum in the THF solution of the compound $[Au\{\eta^2\text{-}Fe_2(CO)_8\}_2]^-$ reveals three main peaks at 2001, 1965 and 1948 cm^{-1}, 10-25 cm^{-1} red shifted compared to the experimental ones. An additional peak is calculated at 1832 cm^{-1} only for the $[Au\{\eta^2\text{-}Fe_2(CO)_8\}\{\eta^2\text{-}Fe_2(CO)_6(\mu\text{-}CO)_2\}]^-$ isomer corresponding to the stretching of the bridging CO ligands.

In previous papers, the bimetallic pentanuclear cluster $[Au\{\eta^2\text{-}Fe_2(CO)_8\}_2]^-$ has been described as formed by two dianionic $\{Fe_2(CO)_8\}^{2-}$ units interacting with a Au(III) center.[30-32] According to the classic Ligand Field (LF)Theory,[19-21] the bonding in the cluster is described as four electron-pair donations from four populated orbital combinations of the two Fe_2 units into the empty orbitals of d^8 Au(III) ion, namely one d, the s and two p ones. The LF Theory is based on the assumption that the ligand-orbitals combinations are lower in energy than the metal orbitals, thus, the LUMO is expected to be mainly centered on the Au, with only a small contribution by the two Fe_2 units, acting as ligands in this case. The bonding in the overall complex is better described as the result of three donations from the Fe_2 units to empty Au orbitals and the fourth interaction is a σ donation from Au to a suitable empty combination of Fe_2 units orbitals. The situation in $[Au\{\eta^2\text{-}Fe_2(CO)_8\}_2]^-$ appears inverted to the LF description as shown in Figure 4, since the Au contribution to the LUMO orbital (σ anti-bonding interaction) is only 7.6 %, while the percentage from the four iron atoms exceeds 64%. This result is in perfectly agreement with the recently

proposed Inverted Ligand Field (ILF) theory.[18] No particular difference has been detected when two CO ligands are bridged, being 10.8 and 63 %, the contributions from the central gold and the four iron centers together, respectively. The involved gold d orbital could be reasonably d_{x2-y2} although some slight differences could be pointed out due to the geometric distortion from the perfect square planar coordination around the gold center. The counterpart bonding combination, mainly centered on the gold, lies very low in energy, being the HOMO-20 molecular orbital (Figure S3). The frontier molecular orbitals for the three redox species, shown in Figure S4, have a very limited contribution from the central gold. Being the five d gold orbitals located at very low energy, they are fully populated, and slightly involved in the reduction processes.
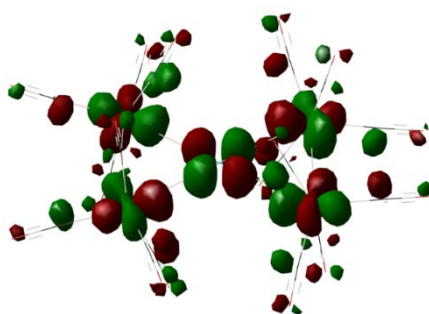

Figure 4. Lowest Unoccupied Molecular Orbital (LUMO) of $[Au\{\eta^2\text{-}Fe_2(CO)_8\}_2]^-$.

The four metal-metal interactions are shown in Figure 5,the first three are ligands (Fe_2 moieties) to metal donations while the fourth represents a metal to ligand σ donation.
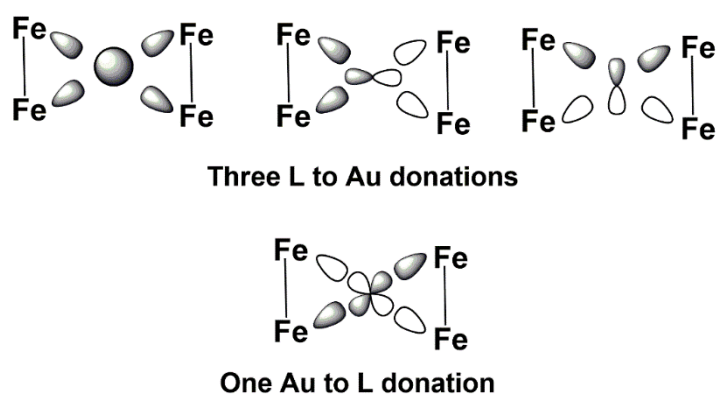

Three L to Au donations

One Au to L donation

Figure 5. Bonding Interaction in $[Au\{\eta^2\text{-}Fe_2(CO)_8\}_2]^-$ between the central gold and the ligands, L, $Fe_2(CO)_8$ units

The aforementioned description allows to conclude that the central gold never attains a d^8 configuration but always maintains its d^{10} electrons at the expenses of the ligands, which are 2 e^- depopulated.

The detailed analysis of the electronic structure provides also a reasonable answer to the pristine dilemma regarding the seventh predicted metal-metal linkage. This should involve a d_{z2} populated orbital of the central Au atom, thus a π–type Au-Fe interaction is expected. In the present case, the latter is absent, reasonably due to the negligible overlap between the d_{z2} orbital and suitable orbital combination of the Fe_2 units. Thus, an additional lone pair is localized on the gold center (at very low energy being HOMO-10) in place of one delocalized M-M bonding, explaining the aforementioned apparent disagreement.

The $[Au\{\eta^2\text{-}Fe_2(CO)_8\}_2]^-$ cluster undergoes two reversible one-electron reduction processes. In this regards, computational analysis could provide some useful hints on which part of the molecule is involved in the electron flow. Two different isomers have been optimized for the mono-reduced radical species $[Au\{\eta^2\text{-}Fe_2(CO)_8\}_2]^{2-}$: a) without and b) with two bridging carbonyl ligands, as shown in Figure 6. The structure with the two CO bridging ligands is more stable by -1.8 kcal mol^{-1} in free energy.
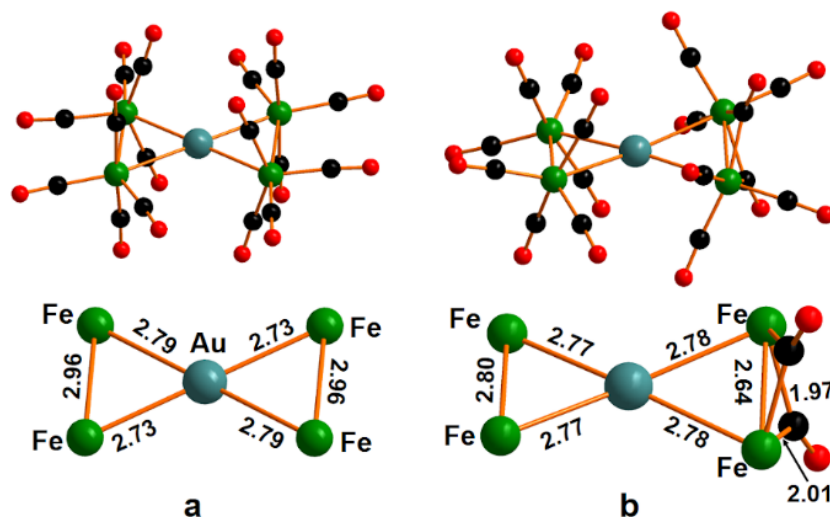

Figure 6. Optimized structure of the reduced form (in the upper part): a) $[Au\{\eta^2\text{-}Fe_2(CO)_8\}_2]^{2-}$ without bridging CO ligands and b) $[Au\{\eta^2\text{-}Fe_2(CO)_8\}\{\eta^2\text{-}Fe_2(CO)_6(\mu\text{-}CO)_2\}]^{2-}$ with two bridging COs. In the lower part, simplified scheme of M-M distance and bridging ligands where available.

From a structural viewpoint, the unbridged isomer still features a *quasi*-planar metal arrangement with an asymmetric elongation of the metal-metal distances, especially for the Fe-Fe linkages. Otherwise, the structure with bridging ligands exhibits a distortion from the planarity being the dihedral angle of the four iron centers 152°. The elongation of the Au-Fe and the Fe-Fe distances is easily understood by looking at the spin density plot of the radical species, shown in Figure 7,perfectly resembling the LUMO in Figure 4 with a greater contribution from the iron centers rather than the central gold one. The negligible involvement of the gold center in the reduction process is another confirmation of the gold d^{10} configuration. The presence of the bridging carbonyl ligands allows asymmetry in the spin density distribution between the two Fe_2 units, being the contribution from the unbridged moiety almost three times bigger than that of the bridged one (0.70 *vs*. 0.26 $e^2/bohr^3$). Such an asymmetry vanishes in the isomer of Figure 6a without bridging ligands, once again highlighting the key-role played by the carbonyl ligands. The addition of a further electron allows the cleavage of one Au-Fe linkage, as shown by the crystallographic structure.
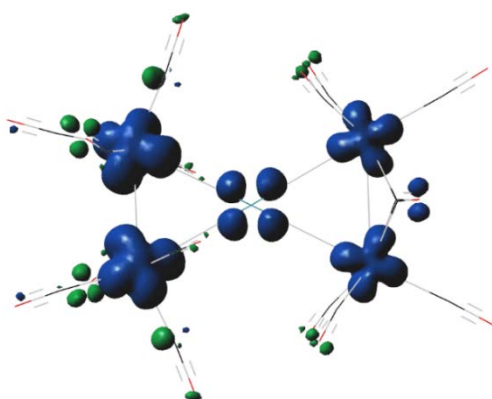

Figure 7. Spin density of the doublet $[Au\{\eta^2-Fe_2(CO)_8\}\{\eta^2-Fe_2(CO)_6(\mu-CO)_2\}]^{2-}$species.

Once again, the presence of the bridging CO ligands causes the appearance of peaks in the 1728-1744 cm^{-1} region in the calculated IR spectrum. These are 15-20 cm^{-1} red-shifted compared to the experimental data, as already found for the starting monoanion.

Two different isomers, with a very small (less than 1.5 kcal mol^{-1}) free energy gap in favor of the bridged structure, have been obtained also for $[Au\{\eta^2-Fe_2(CO)_8\}_2]^{3-}$, as shown in Figure 8. A comparison between the trianionic experimental and the calculated species has been reported in Table S3. In both cases, the structures show a complete cleavage of one(Figure 8b) or two (Figure 8a) Au-Fe linkage(s), in agreement with the complete filling of the LUMO of Figure 4. In the

unbridged structure the Fe-Fe distances remain particularly long (*ca.* 3.0 Å) while the presence of bridging carbonyl allows the shortening of the Fe-Fe linkage.
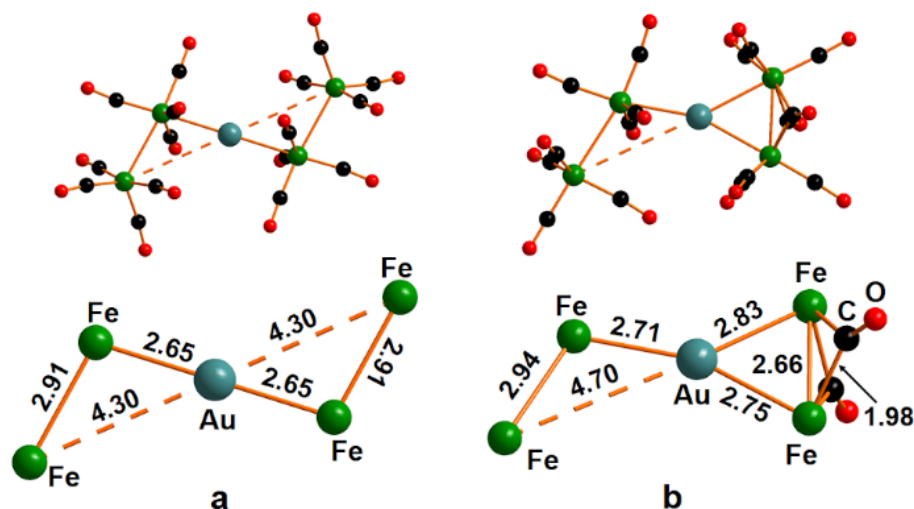

Figure 8. Optimized structure of the bis-reduced form (in the upper part): a) $[Au\{\eta^2\text{-}Fe_2(CO)_8\}_2]^{3-}$ without bridging CO ligands and b) $[Au\{\eta^2\text{-}Fe_2(CO)_8\}\{\eta^2\text{-}Fe_2(CO)_6(\mu\text{-}CO)_2\}]^{3-}$ with two bridging COs. In the lower part, a simplified picture of M-M distance and bridging ligands, where available, is provided.

The computed isomer of Figure 8b satisfactorily reproduces the available X-ray structure of the di-reduced compound, shown in Figure2, featuring the cleavage of the Au-Fe bond, as already predicted by the analysis of the LUMO of Figure 4. From a spectroscopic viewpoint, a further red shift in the carbonyl ligands stretching occurs, confirming the more efficient π metal back-donation from the electron rich Fe centers to the CO ligands.

4   CONCLUSION

A combined experimental/computational approach has provided a new interpretation of the bonding pattern, thus of the redox behavior, of the bimetallic tie-bow carbonyl cluster $[Au\{\eta^2\text{-}Fe_2(CO)_8\}_2]^-$, in the light of the novel concept of the Inverted Ligand Field.[14,18,22] In particular, the central gold, up to now considered as Au(III) and an acceptor of four electron pairs, has been ascertained to have a d^{10} configuration and to behave as a donor of two electrons toward the two Fe$_2$ units. The detailed analysis of the LUMO orbital has revealed a strong contribution from the Fe$_2$ ligands with only a very limited contribution from the central gold, in contrast with the classic Ligand Field theory.[19-21] Thus, the redox processes should mainly involve the Fe$_2$ units rather than

Au, as confirmed by the spectro-electrochemical experiments carried out upon the stepwise reduction of the system. In this regards, a red shift for the carbonyl stretching occurs suggesting a more electron availability at the iron centers, thus a more efficient back-donation towards the CO ligands.

The reversible feature of the two sequential one-electron reduction processes has allowed the isolation of solid-state structure of the di-reduced $[Au\{\eta^1\text{-}Fe_2(CO)_8\}\{\eta^2\text{-}Fe_2(CO)_6(\mu\text{-}CO)_2\}]^{3-}$ featuring a broken Au-Fe linkage. The obtained structural transformation upon reduction is in agreement with the stepwise population of the LUMO orbital in the starting mono-anion species.

This paper represents the first case of ILF concept application to a metal cluster and could provide useful hints for understanding the bonding pattern and electronic distribution in other larger gold clusters up to gold-based nanoparticles.

ASSOCIATED CONTENT

The Supporting Information is available free of charge at https://pubs.acs.org/doi/. The Supporting Information contain the cartesian coordinates and the energy parameters of all the optimized structures.

Accession Codes:

CCDC 2117994 contains the supplementary crystallographic data for this paper. These data can be obtained free of charge via www.ccdc.cam.ac.uk/data_request/cif, or by emailing data_request@ccdc.cam.ac.uk, or by contacting The Cambridge Crystallographic Data Center, 12 Union Road, Cambridge CB2 1EZ, UK; fax: +44 1223 336033.

AUTHOR INFORMATION

Corresponding Authors

Gabriele Manca- Istituto di Chimica dei Composti Organometallici (CNR-ICCOM), 50019, Sesto Fiorentino, Italy. ORCID: https://orcid.org/0000-0003-2068-1731.Email: gabriele.manca@iccom.cnr.it

Maria Carmela Iapalucci - Dipartimento di Chimica Industriale "Toso Montanari", Università di Bologna, Viale Risorgimento 4, 40136 Bologna, Italy. ORCID: https://orcid.org/0000-0001-6955-7999. Email: maria.iapalucci@unibo.it

Authors:

Fabrizia Fabrizi de Biani - Dipartimento di Biotecnologie Chimica e Farmacia and C.I.R.C.M.S.B., Università di Siena Via Aldo Moro, 53100 Siena, Italy.

Maddalena Corsini - Dipartimento di Biotecnologie Chimica e Farmacia and C.I.R.C.M.S.B., Università di Siena Via Aldo Moro, 53100 Siena, Italy; https://orcid.org/0000-0002-5920-5436.

Cristiana Cesari - Dipartimento di Chimica Industriale "Toso Montanari", Università di Bologna, Viale Risorgimento 4, 40136 Bologna, Italy; https://orcid.org/0000-0003-2595-2078.

Cristina Femoni - Dipartimento di Chimica Industriale "Toso Montanari", Università di Bologna, Viale Risorgimento 4, 40136 Bologna, Italy; https://orcid.org/0000-0003-4317-6543.

Stefano Zacchini, Dipartimento di Chimica Industriale "Toso Montanari", Università di Bologna, Viale Risorgimento 4 - 40136 Bologna. Italy. ORCID: https://orcid.org/0000-0003-0739-0518.

Andrea Ienco - Istituto di Chimica dei Composti Organometallici (CNR-ICCOM), 50019 Sesto Fiorentino, Italy; https://orcid.org/0000-0002-2586-4943.

Notes

The authors declare no competing financial interest.

References

(1) Harper, M. J.; Arthur, C. J.; Crosby, J.; Emmett, E. J.; Falconer, R. L.; Fensham-Smith, A. J.; Gates, P. J.; Leman, T.; McGrady, J. E.; Bower, J. F.; Russell, C. A. Oxidative Addition, Transmetallation, and Reductive Elimination at a 2,2'-Bipyridyl-Ligated Gold Center. *J. Am. Chem. Soc.* **2018**, *140,* 4440-4445.

(2) Teles, J. H. Oxidative Addition to Gold(I): A new Avenue in Homogeneous Catalysis with Au. *Angew. Chem. Int. Ed.* **2015**, *54*, 5556-5558.

(3) Rodriguez, J.; Tabey, A.; Mallet-Ladeira, S.; Bourissou, D. Oxidative additions of alkynyl/vinyl iodides to gold and gold-catalyzed vinylation reactions triggered by the MeDalphos ligand. *Chem. Sci.* **2021**, *12*, 7706-7712.

(4) Rigoulet, M.; Thillaye du Boullay, O.; Amgoune, A.; Bourissou, D. Gold(I)/Gold(III) Catalysis that Merges Oxidative Addition and π-Alkene Activation. *Angew. Chem.* **2020**, *132*, 16768-16773.

(5) Joost, M.; Zeineddine, A.; Estevez, L.; Mallet-Ladeira, S.; Miqueu, K.; Amgoune, A.; Bourissou, D. Facile Oxidative Addition of Aryl Iodides to Gold(I) by Ligand Design: Bending Turns on Reactivity. *J. Am. Chem. Soc.* **2014**, *136*, 14654–14657.

(6) Komiya, S.; Albright, T. A.; Hoffmann, R.; Kochi, J. K. Reductive Elimination and Isomerization of Organogold Complexes. Theoretical Studies of Trialkyl gold Species as Reactive Intermediates. *J. Am. Chem. Soc.* **1976**, *98*, 7255−7265.

(7) Messori, L.; Macron, G.; Orioli, P. Gold (III) Compounds as New Family of Anticancer Drugs. *Bioinorg. Chem. Appl.* **2003**, *1*, 177-187.

(8) Giorgio, A.; Merlino, A. Gold metalation of proteins: Structural studies. *Coord. Chem. Rev.* **2020**, *407*, 213175.

(9) Tong, K.-C.; Lok, C.-N.; Hu, D.; Fung, Y. M. E.; Chang, X.-Y.; Huang, S.; Jiang, H.; Che, C.-M. An anticancer gold (III)-activated porphyrin scaffold that covalently modifies protein cysteine thiols. *PNAS* **2020**, *117*, 1321-1329.

(10) Saha, K.; Agasti, S. S.; Kim. C.; Li, X.; Rotello, V. Gold Nanoparticles in Chemical and Biological Sensing.*Chem. Rev.* **2012**, *112*, 2739-2779.

(11) Nosratabad, N. A.; Jin, Z.; Du, L.; Thakur, M.; Mattoussi, H. N-Heterocyclic Carbene-Stabilized Gold Nanoparticles: Mono- Versus Multidentate Ligands. *Chem. Mat.* **2021**,*33*, 921-933.

(12) Nath, P.; Priyadarshni, N.; Mandal, S.; Singh, P.; Arun, R. K.; Chanda, N. Gold Nanostruture in Sensor Technology: Detection and Estimation of Chemical Pollutants. *Environmental, Chemical and Medicinal Sensors,* **2017**, 31-66.

(13) Romine, A. M.; Nebra, N.; Konovalov, A. I.; Martin, E.; Benet-Buchholz, J.; Grushin, V. V. Easy Access to the Copper(III) Anion$[Cu(CF_3)_4]^-$.*Angew. Chem., Int. Ed.* **2015**,*54*, 2745−2749.

(14) Walroth, R. C.; Lukens, J. T.; MacMillan, S. N.; Finkelstein, K.D.; Lancaster, K. M. Spectroscopic Evidence for a 3d^{10} Ground State Electronic Configuration and Ligand Field Inversion in [Cu(CF$_3$)$_4$]$^{1-}$. *J. Am. Chem. Soc.* **2016**, *138*, 1922−1931.

(15) Gao, C.; Macetti, G.; Overgaard, J. Experimental X-ray Electron Density Study of Atomic Charges, Oxidation States, and Inverted Ligand Field in Cu(CF$_3$)$_4^-$. *Inorg. Chem.* **2019**, *58*, 2133-2139.

(16) Snyder, J. P. Distinguishing Copper d^8 and d^{10} Configurations in a Highly Ionic Complex; A Nonformal Metal Oxidation State. *Angew. Chem., Int. Ed. Engl.* **1995**, *34*, 986−987.

(17) Kaupp, M.; von Schnering, H. G. Formal Oxidation State versus Partial Charge-A Comment.*Angew. Chem., Int. Ed. Engl.* **1995**,*34*, 986.

(18) Hoffmann, R.; Alvarez, S.; Mealli, C.; Falceto, A.; Cahill III, T. J.; Zeng, T.; Manca, G. From Widely Accepted Concepts in Coordination Chemistry to Inverted Ligand Fields *Chem. Rev.* **2016**, *116,* 8173-8192.

(19) Figgis, H. B. N. *Introduction to Ligand Fields.* John Wiley & Sons Ltd., London and New York 1966. 361. Seiten. Preis: 72/-. **1966**, *70*, 932-933.

(20) Albright, T. A.; Burdett, J. K.; Whangbo, M. H. Orbital Interactions in Chemistry Wiley-Interscience; 2nd edition, **2013**.

(21) Cirera, J.; Alvarez, S. How High the Spin? Allowed andForbidden Spin States in Transition-Metal Chemistry. *Angew. Chem.,Int. Ed.* **2006**, *45*, 3012−3020.

(22) DiMucci, I. M.; Lukens, J. T.; Chatterjee, S.; Carsch, K. M.; Titus, C. J.; Lee, S. J.; Nordlund, D.; Betley, T. A.; MacMillan, S. N.; Lancaster, K. M. The Myth of d^{8}Copper(III). *J. Am. Chem. Soc.* **2019**, *141*, 18508−18520.

(23) Perez-Bitrian, A.; Baya, M.; Casas, J. M.; Martin, A.; Menjon, B. Hydrogen bonding to metals as a probe for an inverted ligand field. *Dalton Trans.* **2021**, *50*, 5465-5472.

(24) Baya, M.; Joven-Sancho, D.; Alonso, P. J.; Orduna, J.; Menjon, B. M−C Bond Homolysis in Coinage-Metal [M(CF$_3$)$_4$]$^-$ Derivatives. *Angew. Chem., Int. Ed.* **2019**, *58*, 9954-9958.

(25) Martinez-Salvador, S.; Falvello, L. R.; Menjon, B. Gold(I) and Gold(III) Trifluoromethyl Derivatives. *Chem. –Eur. J.* **2013**, *19*, 14540-14552.

(26) Ciabatti, I.; Femoni, C.; Iapalucci, M. C.; Ienco, A.; Longoni, G.; Manca, G.; Zacchini, S. Intramolecular d^{10}–d^{10} Interactions in a Ni$_6$C(CO)$_9$(AuPPh$_3$)$_4$ Bimetallic Nickel–Gold Carbide Carbonyl Cluster. *Inorg. Chem.* **2013**, *52*, 10559-10565.

(27) Ciabatti, I.; Femoni, C.; Hayatifar, M.; Iapalucci, M. C.; Ienco, A.; Longoni, G.; Manca, G.; Zacchini, S. Octahedral Co-Carbide Carbonyl Clusters Decorated by $[AuPPh_3]^+$ Fragments: Synthesis, Structural Isomerism, and Aurophilic Interactions of $Co_6C(CO)_{12}(AuPPh_3)_4$. *Inorg. Chem.* **2014**, *53*, 9761-9770.

(28) Cesari, C.; Shon, J.-H.; Zacchini, S.; Berben, L. A. Metal Carbonyl Clusters of Group 8-10: Synthesis and Catalysis, *Chem. Soc. Rev.* **2021**, *50*, 9503-9539.

(29) Ciabatti, I.; Femoni, C.; Iapalucci, M. C.; Ruggieri, S.; Zacchini, S. The role of gold in transition metal carbonyl clusters. *Coord. Chem. Rev.* **2018**, *355*, 27-38.

(30) Albano, V. G.; Monari, M.; De Martin, F.; Macchi, P.; Femoni, C.; Iapalucci, M. C.; Longoni, G. Synthesis and chemical behavior of $[MFe_4(CO)_{16}]^{n-}$ (M=Au, Zn, Cd, Hg) clusters: X ray structure of $[NMe_3CH_2Ph]_2[Au\{Fe_2(CO)_8\}_2]Cl$ and $[PPh_4]_2[Cd\{Fe_2(CO)_6(\mu-CO)_2\}_2]\cdot2CH_3CN$ *Solid State Sciences* **1999**, 597-606.

(31) Albano, V. G.; Aureli, R.; Iapalucci, M. C.; Laschi, F.; Longoni, G.; Monari, M.; Zanello, P. Synthesis, Characterization and Electrochemical Behaviour of the $[Fe_4Au(CO)_{16}]^{n-}$ (n=1,2,3) Clusters. X-Ray Structure of $[NMe_3CH_2Ph]_2[Fe_4Au(CO)_{16}]Cl$. *J. Chem. Soc., Chem. Commun.* **1993**, 1501-1502.

(32) Femoni, C.; Iapalucci, M. C.; Longoni, G.; Tiozzo, C.; Wolowska, J.; Zacchini, S.; Zazzaroni, E. New Hybrid Semiconductor Materials Based on Viologen Salts of Bimetallic Fe-Pt and Fe-Au Carbonyl Clusters: First Structural Characterization of the Diradical π-Dimer of the Diethylviologen Monocation and EPR Evidence of its Triplet State. *Chem. Eur. J.* **2007**, *13*, 6544-6554.

(33) Bonelli, R.; Zacchini, S.; Albonetti, S. Gold/Iron carbonyl Clusters for Tailored Au/FeO_x Supported Catalysts. *Catalysts* **2012**, *2*, 1-23.

(34) Vinogradov, M. M.; Nelyubina, Y. V.; Corsini, M.; Fabrizi de Biani, F.; Kudinov, A. R.; Loginov, D. A. Thioether Iron Complexes $[(X-SMe-7,8-C_2B_9H_{10})Fe(C_6H_6)]$ (X = 9 or 10) as Synthons of Neutral Ferracarborane Fragments. *Eur. J. Inorg. Chem.* **2017**, 4627-4634.

(35) Sheldrick, G. M. Crystal Structure Refinement with SHELXL. *Acta Crystallogr., Sect. C: Struct. Chem.* **2015**, *C71*, 3-8.

(36) Becke, A. D. Density-functional thermochemistry. III. The role of exact exchange *J. Chem. Phys.* **1993**, *98*, 5648-5652.

(37) Gaussian 16, Revision C.01, Frisch, M. J.; Trucks, G. W.; Schlegel, H. B.; Scuseria, G. E.; Robb, M. A.; Cheeseman, J. R.; Scalmani, G.; Barone, V.; Petersson, G. A.; Nakatsuji, H.; Li, X.; Caricato, M.; Marenich, A. V.; Bloino, J.; Janesko, B. G.; Gomperts, R.; Mennucci, B.; Hratchian, H. P.; Ortiz, J. V.; Izmaylov, A. F.; Sonnenberg, J. L.; Williams-Young, D.; Ding, F.; Lipparini, F.; Egidi, F.; Goings, J.; Peng, B.; Petrone, A.; Henderson, T.; Ranasinghe, D.; Zakrzewski, V. G.; Gao, J.; Rega, N.; Zheng, G.; Liang, W.; Hada, M.; Ehara, M.; Toyota, K.; Fukuda, R.; Hasegawa, J.; Ishida, M.; Nakajima, T.; Honda, Y.; Kitao, O.; Nakai, H.; Vreven, T.; Throssell, K.; Montgomery, J. A., Jr.; Peralta, J. E.; Ogliaro, F.; Bearpark, M. J.; Heyd, J. J.; Brothers, E. N.; Kudin, K. N.; Staroverov, V. N.; Keith, T. A.; Kobayashi, R.; Normand, J.; Raghavachari, K.; Rendell, A. P.; Burant, J. C.; Iyengar, S. S.; Tomasi, J.; Cossi, M.; Millam, J. M.; Klene, M.; Adamo, C.; Cammi, R.; Ochterski, J. W.; Martin, R. L.; Morokuma, K.; Farkas, O.; Foresman, J. B.; Fox, D. J. Gaussian, Inc., Wallingford CT, 2016.

(38) Barone, V.;Cossi, M. Quantum Calculation of Molecular Energies and Energy Gradients in Solution by a Conductor Solvent Mode. *J. Phys. Chem. A* **1998**, 102, 1995−2001.

(39) Cossi, M.; Rega, N.; Scalmani, G.; Barone, V. Energies, structures, and electronic properties of molecules in solution with the C-PCM solvation model. *J. Comput. Chem.* **2003**, *24*, 669−681.

(40) Schaefer, A.; Huber, C.; Alrichs, R. Fully optimized contracted Gaussian-basis sets of triple zeta valence quality for atoms Li to Kr. *J. Chem. Phys.* **1994**, *100,*5829-5835.

(41) Dolg, M.; Stoll. H.; Preuss, H.; Pitzer, R. M. Relativistic and correlation effects for element 105 (hahnium, Ha): a comparative study of M and MO (M = Nb, Ta, Ha) using energy-adjusted ab initio pseudopotentials *J. Phys. Chem.* **1993**, *97*, 5852−5859.

(42) Gorelsky, S. I. *AOMix: Program for Molecular Orbital Analysis*, http://www.sg-chem.net/, version 6.94, 2019.

(43) Gorelsky, S. I.; Lever, A. B. P. Electronic structure and spectra of ruthenium diimine complexes by density functional theory and INDO/S. Comparison of the two methods. *J. Organomet. Chem.* **2001**, *635*, 187-196.

(44) MacLaughlin, S. A.; Taylor, N. J.; Carty, A. J. $Ru_5(CO)_{16}(\mu\text{-}PPh_2)(\mu^5\text{-}P)$: a low-nuclearity cluster with a partially encapsulated phosphide. *Inorg. Chem.* **1983**, *22*, 1409-1411.

(45) Berti, B.; Bortoluzzi, M.; Cesari, C.; Femoni, C.; Iapalucci, M. C.; Mazzoni, R.; Vacca, F.; Zacchini, S. Thermal Growth of Au-Fe Heterometallic Carbonyl Clusters Containing N-Heterocyclic Carbene and Phosphine Ligands. *Inorg. Chem.* **2020**, *59*, 2228-2240.

(46) Berti, B.; Bortoluzzi, M.; Cesari, C.; Femoni, C.; Iapalucci, M. C.; Mazzoni, R.; Vacca, F.; Zacchini, S. Polymerization Isomerism in $[\{MFe(CO)_4\}_n]^{n-}$ (M = Cu, Ag, Au; N 0 = 3, 4) Molecular Clusters Supported by Metallophilic Interactions. *Inorg. Chem.* **2019**, *58*, 2911-2915.

(47) Bortoluzzi, M.; Cesari, C.; Ciabatti, I.; Femoni, C.; Hayatifar, M.; Iapalucci, M. C.; Mazzoni, R.; Zacchini, S. Bimetallic Fe-Au Carbonyl Clusters Derived from Collman's Reagent: Synthesis, Structure and DFT Analysis of $Fe(CO)_4(AuNHC)_2$ and $[Au_3Fe_2(CO)_8(NHC)_2]^-$. *J. Clust. Sci.* **2017**, *28*, 703-723.

(48) Bruce, M. I. Pentanuclear ruthenium clusters containing C_2 and related ligands *J. Clus. Science* **1997**, *8*, 293-327.

(49) Ceriotti, A.; Daghetta, M.; El Afefey, S.; Ienco, A.; Longoni, G.; Manca, G.; Mealli, C.; Zacchini, S.; Zarra, S. Electronic Stabilization of Trigonal Bipyramidal Clusters: the Role of the Sn(II) Ions in $[Pt_5(CO)_5\{Cl_2Sn(\mu-OR)SnCl_2\}_3]^{3-}$ (R = H, Me, Et, ^{i}Pr). *Inorg. Chem.* **2011**, *50*, 12553-12561.

(50) Farrar, D. H.; Johnson, B. F. G.; Lewis, J.; Raithby, P. R.; Rosales, M. J. Preparation and some reactions of $[Os_5(CO)_{19}]$; the molecular structures of $[Os_5(CO)_{19}]$ and $[Os_5(CO)_{16}\{P(OMe)_3\}_3]$. *J. Chem. Soc., Dalton Trans.* **1982**, 2051-2058.

(51) Mealli, C.; Proserpio, D. M. Intermetal Bonding Network in Two-Dimensional Tetranuclear Clusters. *J. Am. Chem. Soc.* **1990**, *112*, 5484-5496.

(52) Mealli, C.; Lopez, J. A.; Sun, Y.; Calhorda, M. J. MO architectures of octahedral metal clusters. *Inorg. Chim. Acta* **1993**, *213*, 199-212.

(53) Hirva, P.; Haukka, M.; Jakonen, M.; Moreno, M. A. DFT tests for group 8 transition metal carbonyl complexes. *J. Mol. Mod.* **2008**, *14*, 171-181.

(54) Lombardi, J. R.; Davis, B. Periodic Properties of Force Constants of Small Transition-Metal and Lanthanide Clusters. *Chem. Rev.* **2002**, *102*, 2431-2460.

Table of Contents

Au d^8 or Au d^{10}?
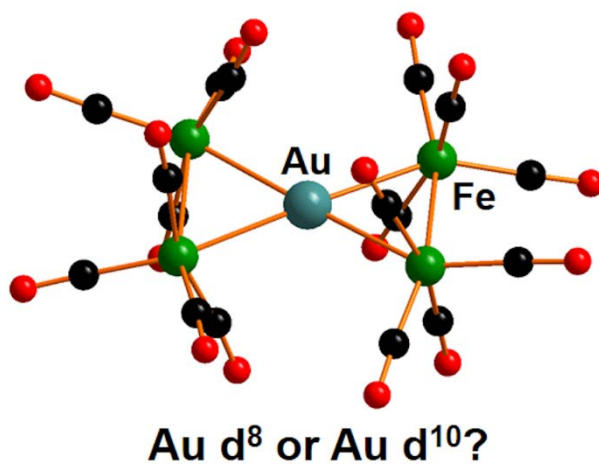
In contrast to the classical view, the electronic configuration of the central gold in a penta-nuclear tie bow cluster does not significantly change during the electrochemical reductions, which mainly involve the Fe$_2$ units. Spectroelectrochemical and X-ray studies support such a new interpretation based on the Inverted Ligand Field (ILF) Framework.